

3-D seismic structure of the Kachchh, Gujarat, and its implications for the earthquake hazard mitigation

A. P. Singh · O. P. Mishra · B. K. Rastogi · Dinesh Kumar

Received: 14 January 2010 / Accepted: 26 December 2010 / Published online: 18 January 2011
© Springer Science+Business Media B.V. 2011

Abstract Several pieces of studies on the January 26, 2001, Bhuj earthquake (Mw 7.6) revealed that the mainshock was triggered on the hidden unmapped fault in the western part of Indian stable continental region that caused a huge loss in the entire Kachchh rift basin of Gujarat, India. Occurrences of infrequent earthquakes of Mw 7.6 due to existence of hidden and unmapped faults on the surface have become one of the key issues for geoscientific research, which need to be addressed for evolving plausible earthquake hazard mitigation model. In this study, we have carried out a detailed autopsy of the 2001 Bhuj earthquake source zone by applying three-dimensional (3-D) local earthquake tomography (LET) method to a completely new data set consisting of 576 local earthquakes recorded between November 2006 and April 2009 by a seismic network consisting of 22 numbers of three-component broadband digital seismograph stations. In the present study, a total of 7560 arrival times of P-wave (3820) and S-wave (3740) recorded at least 4 seismograph stations were inverted to assimilate 3-D P-wave velocity (V_p), S-wave velocity (V_s), and Poisson's ratio (σ) structures beneath the 2001 Bhuj earthquake source zone for reliable interpretation of the imaged anomalies and its bearing on earthquake hazard of the region. The source zone is located near the triple junction formed by juxtapositions of three Indian, Arabian, and Iranian tectonic plates that might have facilitated the process of brittle failure at a depth of 25 km beneath the KRB, Gujarat, which caused a gigantic loss to both property and persons of the region. There may be several hidden seismogenic faults around the epicentral zone of the 2001 Bhuj earthquake in the area,

A. P. Singh (✉) · B. K. Rastogi
Institute of Seismological Research (ISR), Raisan, Gandhinagar, Gujarat, India
e-mail: apsingh07@gmail.com

O. P. Mishra
Geological Survey of India (GSI), 27, J. L. Nehru Road, Kolkata, West Bengal, India

Present Address:

O. P. Mishra
SAARC Disaster Management Centre, New Delhi, India

D. Kumar
Department of Geophysics, Kurukshetra University, Kurukshetra, Haryana, India

which are detectable using 3-D tomography to minimize earthquake hazard for a region. We infer that the use of detailed 3-D seismic tomography may offer potential information on hidden and unmapped faults beneath the plate interior to unravel the genesis of such big damaging earthquakes. This study may help in evolving a comprehensive earthquake risk mitigation model for regions of analogous geotectonic settings, elsewhere in the world.

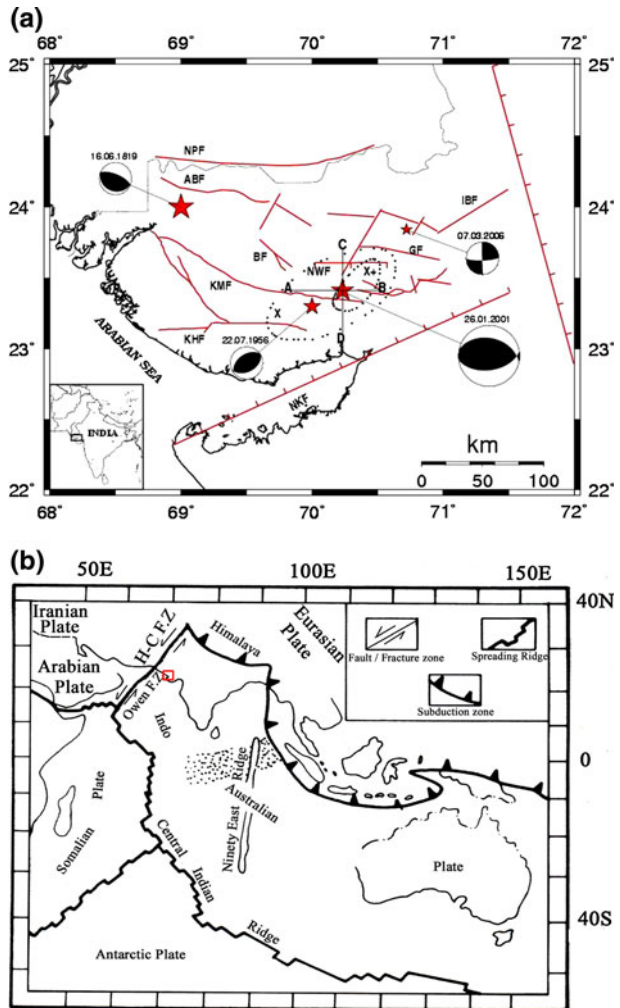
Keywords Earthquake hazard · Arabian Sea · Seismic tomography · Sea water · Permeation · The 2001 Bhuj earthquake

1 Introduction

The devastating Bhuj earthquake (M_w 7.6) occurred on the early morning (08 h 46 min, IST) of January 26, 2001, in the Kachchh rift basin (KRB) in the Gujarat province of western margin of peninsular India (Fig. 1a–b) rocked the whole country, killed about 20,000 people, and destroyed over 4,00,000 buildings (Rajendran et al. 2001). The Bhuj earthquake region lie in zone V, which is the highest hazard seismic zoning in the map of India and has potential for M 8 earthquakes (Bureau of Indian Standards 2002). The epicenter of the earthquake was reported at 23.412°N and 70.232°E with focal depth at 25 km (Rastogi et al. 2001; Negishi et al. 2002; Mishra and Zhao 2003; Mandal et al. 2004a). A maximum intensity of X+ on the modified Mercalli [MMI] scale was assigned by Rastogi et al. 2001. The fault plane solution of the mainshock of the Bhuj earthquake indicated a reverse faulting with a strike-slip component (Kayal et al. 2002) similar to that of 1956 Anjar earthquake (Chung and Gao 1995). The mainshock rupture did not reach to the surface (Talwani and Gangopadhyay 2001; Mishra and Zhao 2003; Mandal et al. 2004a; Mandal and Pujol 2006; Mishra et al. 2008). Surprisingly, the earthquake did not create obvious surface displacements for the main faults, although there were some small surface deformations attributed to shaking effects. Thus, the earthquake indicted several unique features to reckon compared to other large crustal earthquakes particularly in short areal extent of the causative fault at the deeper layer (Negishi et al. 2002). Several theories and hypothesis have been proposed by numerous geological and geophysical investigations to explain the genesis of intraplate earthquakes and its continued aftershocks activity but it is still undiscovered.

The KRB was one among the three major pre-continental rifts, Kachchh, Cambay, and Narmada, that were formed during India separation from the eastern Gondwanaland in early cretaceous. These rift basins originated in different time periods during the Mesozoic. The Kachchh basin rifted during Triassic, Cambay during early Cretaceous, and Narmada during late Cretaceous. These basins received Mesozoic and Cenozoic sediments (Biswas 1987). Figure 1a shows the seismotectonics map of the Gujarat region. There are large east–west (EW) trending features that cross the Kachchh peninsula. These features along with the current configuration of plate motion suggest a north–south (NS) compressional stress field. One of the most important characteristics of the Kachchh region is the occurrence of large but infrequent earthquake. Based on the radiocarbon age data, it has been inferred that a series of earthquakes resulted in this region between 885 and 1035 A.D (Rajendran and Rajendran 2001). In 1668, a larger earthquake occurred in the region with epicenter at (24.0°N, 68.0°E) and a great one was that of Rann of Kachchh earthquake of June 16, 1819 (24.250 N, 69.250 E, M_w 7.8.), that took a toll of about 1,500 people and threw up a 80–90-km ridge and created what is known as Allah Bund, a burning example of major tectonic upheavals due to earthquakes in the region (Rajendran and Rajendran 2001; Gaur 2001). The moment

Fig. 1 a The map showing geotectonic setting of the Kachchh rift basin. The 2001 Bhuj mainshock epicenter and past historical damaging earthquakes are shown by *red stars*. Their respective fault plane solutions are also shown in equal area projection with *white (tension)* and *black (compression)* shades. Faults causing past seismicity in Kachchh region are marked in the figure as: *KMF* Kachchh Mainland Fault, *KHF* Katrol Hill Fault, *ABF* Allah Bund Fault, Old *ABF*; *IBF* Island Belt Fault, *GF* Gedi Fault, *BF* Banni Fault, *NWF* North Wagad Fault, *NPF* Nagar Parkar Fault, *NKF* North Kathiawar Fault. Elliptical areas show distribution of the intensity values *X* and *X⁺* during the 2001 Bhuj earthquake. The *two solid gray lines, AB and CD*, indicate locations of the cross-sections. **b** Map showing a broader view of regional tectonics of India. The *red rectangle* represents the 2001 Bhuj earthquake region



magnitude of the 1819 Kachchh earthquake was estimated to be 7.8 (Johnston 1994). The focal mechanism of Kachchh earthquakes, such as the 1956 Anjar earthquake, 1819 Rann of Kachchh earthquake and few others associated with reverse faulting (Gaur 2001), suggests compressive stress field, caused by the northward collision of the Indian plate with Eurasia since 40 million years ago. Nevertheless, the pre-existing normal faults associated with the possible plume related to early Mesozoic rifting may be getting reactivated as reverse faults, suggesting inverse tectonics (Biswas 1987; Chung and Gao 1995; Rastogi et al. 2001). It is generally believed that the co-seismic uplift evidenced by the Allah Bund is the expression of a fault. The crustal blocks to the south and north of Allah Bund Fault are identified as hanging wall and footwall, respectively (Gaur 2001). A scarp excavated identified in a shallow trenches across this structure has been noted as part of a fold (Rajendran and Rajendran 2001; Gaur 2001), which resulted in progressive migration of streams toward and formation of a lake at the down dip side of the up-thrust block. Between 1821 and 2009, 26 moderate earthquakes of magnitude ranges from 4.2 to 6.1 are reported to have occurred in this region (Rajendran and Rajendran 2001, Institute of Seismological Research (ISR) report 2009). The

last damaging earthquake in this region, prior to the 2001 Bhuj earthquake, was the Anjar earthquake of July 21, 1956, of Mw 6.1 that caused 115 deaths. It is clear from the above descriptions that the present Kachchh study region is one of the most seismically active areas of the India and prone to more seismic hazard, which need to be studied for generating earthquake hazard mitigation parameters for evolving a comprehensive earthquake hazard mitigation model for the region.

Three-dimensional (3-D) local earthquake tomography (LET) is the latest technique for imaging subsurface structure beneath both seismically more active and less active plate interior regions. Several meritorious studies using 3-D tomography have already been carried out for different regions in the world (Aki and Lee 1976; Thurber 1983; Eberhart-Phillips 1986; Zhao et al. 1992; Zhao and Kanamori 1992; Serrano et al. 1998; Mishra and Zhao 2003; Salah and Zhao 2003; Mandal et al. 2004a; Mandal and Pujol 2006; Mukhopadhyay et al. 2006; Salah et al. 2007; Mandal and Chadha 2008). Detailed 3-D tomographic imaging has been successful in understating the mechanism of earthquake initiation, its rupture propagation and cessation, and in imaging the complex crustal structures beneath study region that may shed an important light on the role of hidden faults and its bearing on degree of geohazard in the stable continental region (Zhao et al. 2004).

In the present study, an attempt is made to evaluate three-dimensional (3-D) seismic velocity (V_p and V_s) and Poisson's ratio (σ) structures using a total of 7,560 direct P- and S-wave arrival times generated from a total of 576 aftershock events recorded by 22 broadband seismographs set up in a well-defined network as shown in Fig. 2. This endeavor may shed an important light on the nature and extent seismic heterogeneities beneath the KRB and their control on earthquake initiation, which has direct bearing on degree of geohazard of the region.

2 Geology and tectonic settings of the source zone

The geologic structure and tectonic settings of the KRB and in particular of the 2001 Bhuj earthquake region is the most important to know as the hypocenter located far away from the plate boundary (Fig. 1b). Thus, the occurrence of large earthquakes in the stable continental region of western Indian Peninsula is still a puzzle for geoscientists, which makes seismologists more keen to know causes for nucleating such devastating plate interior earthquake at a depth of 25 km amidst of heterogeneous crustal layers.

Geologically, Quaternary/Cenozoic sediments, Deccan volcanic rocks, and Jurassic sandstones rest on the Archean basement (Biswas 1987; Gupta et al. 2001). While the earthquake epicentral region is composed of Mesozoic rocks (135–65 million years old) and Cenozoic sediments (~ 2 –6 km thick) lying over an uplifted granite basement (Biswas 1987; Gupta et al. 2001). The adjacent area in the south is covered by Deccan volcanic rocks of the southern Kachchh region. The bordering coastal plains are composed of narrow strips of gently dipping Cenozoic sediments. The damage pattern of Kachchh Peninsula is controlled by the geomorphic features. The complex structure and rugged hilly terrain composed of Mesozoic rocks and low-lying plains are parallel to each other. The surface reliefs, sea level changes and process of erosion and deposition are partly controlled by them and ongoing tectonics. Folds, faults, and lineaments mark the geomorphology of the region known to be tectonically active since Mesozoic times, resulting in the creation of new faults, changes in drainage patterns, etc.

Major structural features of the Kachchh region include several EW trending faults/folds. The rift zone is bounded by a south-dipping Nagar Parkar Fault (NPF) in the north

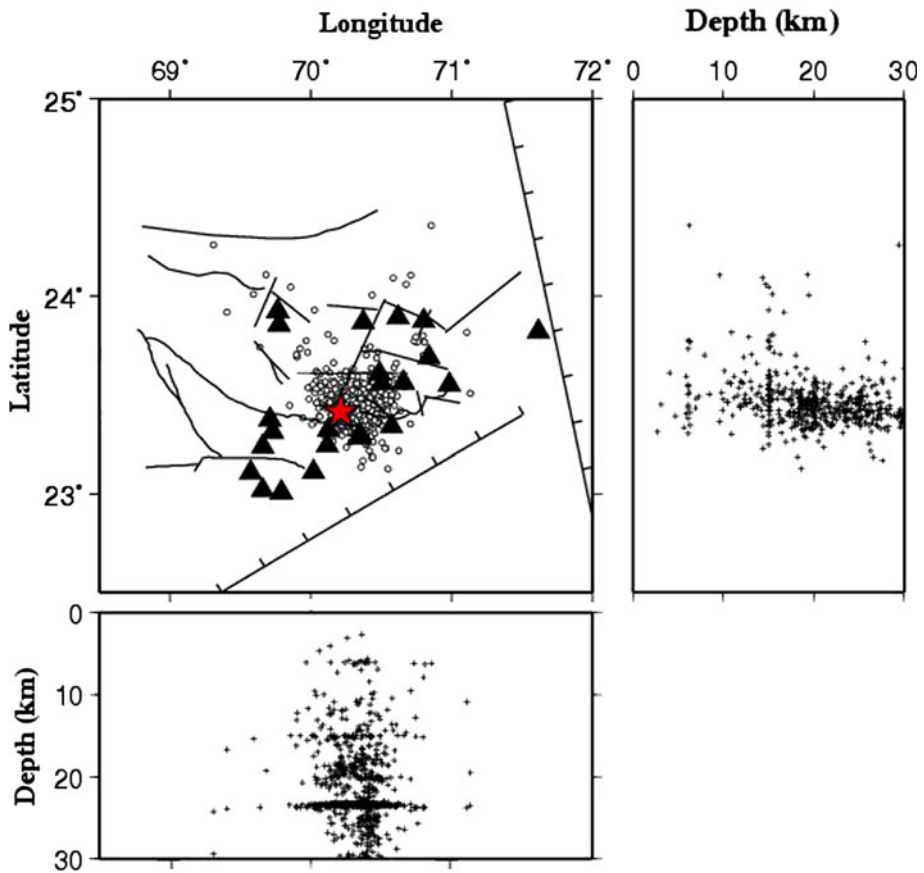


Fig. 2 Epicentral distribution of earthquakes and seismic stations used in this study area is shown by *open circles* and *solid triangles*, respectively, in cross-sectional views with depth (the *left side* shows the distribution of events along latitude with depth, while the *lower one* shows the distribution along longitude with depth). The figure also shows the identified faults of the regions as denoted in Fig. 1a. Depth distribution of the used events (in *crosses*) in the latitude and longitude directions, respectively

and a north-dipping Kathiawar Fault in the south. Other major faults in the region are the EW trending Allah Bund Fault (ABF), Island Belt Fault (IBF), Kachchh Mainland Fault (KMF), and Katrol Hill Fault (KHF) (Fig. 1a). Additionally, several northeast (NE) and northwest (NW) trending small faults/lineaments are also reported. A group of EW trending uplifts namely Kachchh Mainland Uplift, Pachham, Khadir Bela, Wagad and Chobari uplift surrounded by the depressions like the Banni plain and Rann of Kachchh mainly characterize the structural features of the Kachchh rift basin (Biswas 1987). The basement unwrapping/volcanic plugs are associated with positive Bouguer gravity anomalies (Chandrasekhar and Mishra 2002).

3 Data source

After the devastating 2001 Bhuj earthquake many of the premier seismological institutes of India and abroad (e.g., Geological Survey of India, National Geophysical Research

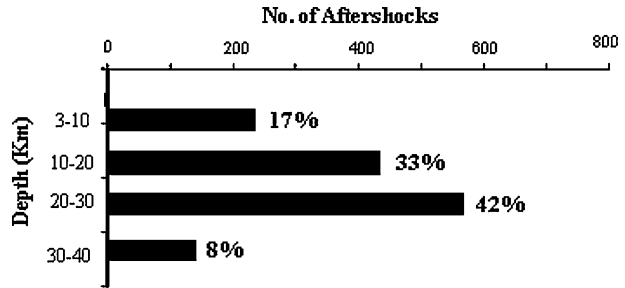
Institute; some research institutions of Japan and USA) had actively indulged in seismological monitoring of aftershocks in the source area by deploying their own seismic network there. However, their monitoring was based on isolation using lesser numbers of seismograph stations with individual seismic network. Our present study deals with relatively comprehensive data recorded by a large number of seismograph stations. Since July 2006, Institute of Seismological Research (ISR), Gandhinagar, Gujarat, India, has installed 50 broadband seismograph (BBS) and 46 strong-motion accelerographs (SMA) covering the whole Gujarat state. Data of 19 broadband stations are brought on real time through VSAT (very small aperture terminal) to data center of ISR. The online data from those stations are available in Guralp format (GCF). The data of Reftech and Geon format are collected from temporary stations. The BBS data are recorded with 50 samples per second (sps) and SMA with 100 sps. However, the SMA data are in trigger mode, having triggering level 0.0195 g.

Arrival times of P- and S-phases are picked up precisely from these waveforms. We have a dense description of seismic rays in lateral and vertical direction for a given source station geometry in the source zone (Fig. 2), which can give us a resolvable seismic structure of the regions. In this study, 576 precisely located events were considered for tomographic inversion. These events were recorded during the period from November 2006 to April 2009. Each event was recorded at least 4 seismic stations and maximally by 22 seismic stations ascribed to the ISR and National Geophysical Research Institute (NGRI). It should be noted that all BBS stations are not installed at once. The epicenter map of 576 events is shown in Fig. 2 from which phase data are extracted for 3-D tomography study.

4 Data analyses and resolution

As mentioned earlier, the arrival time data are generated by aftershocks of magnitude ≥ 1 recorded during November 2006–April 2009 for this study. Most of the events are located within the seismic network. Initially, Hypo71 location tool was used to estimate hypocenters of aftershocks. Then, the aftershocks are relocated with reference to 3-D velocity model simultaneously as shown in Fig. 2. The reliable and accurate aftershock data exhibit E-W trending hidden fault named as the North Wagad Fault (NWF) about 25 km north of the Kachchh Mainland Fault (KMF), initially regarded as the responsible fault for the 2001 Bhuj earthquake (Rastogi et al. 2001; Mandal et al. 2004a, b). It is also found that the majority of the aftershocks are confined between the KMF and NWF (Fig. 1). The selection of events is based on the number of stations (4–22) involved for recording the particular events as well as root mean square (RMS) residual (0.18). We found that errors in depth remained maximum 2.8 km for all events, while epicenter locations (latitude and longitude) have error varying between 0.5 and 1.5 km. Most of the aftershocks have occurred in the depth range of 20–25 km and at distances from 30 to 100 km. These 576 aftershocks generated a total of 3,820 P- and 3,740 S-wave arrivals recorded by our network consisting of 22 seismic stations. The approximately equal number of both P- and S-phase data ensures better distribution of seismic rays, and good crisscrossing in most parts of the study area has an important significance about the reliability of the obtained velocity and Poisson's ratio structures (Widiyantoro et al. 1999; Gorbatov and Kennett 2003). The resolution of tomography is primarily dictated by the quality of the seismic data rather than its quantity for a given set of model parameterization of the area (Zhao et al. 2001). The accuracy of arrival times picks for both P- and S-wave varies from 0.1 to 0.25

Fig. 3 A plot showing histogram of focal depth distribution of the events used in the present study for the 2001 Bhuj earthquake region



for most of the data and slightly higher (0.2–0.3 s) for the events recorded at epicentral distance greater than 200 km. The number of events versus depth is plotted in Fig. 3, which shows that the maximum number of events occurred at a depth range of 20–30 km. It has been suggested by many authors that the depth up to which 90% of the earthquakes occur is the base of the seismogenic zone (Sibson 1989; Lay and Wallace 1995). They have also suggested that larger-magnitude earthquakes tend to nucleate at the base of the seismogenic zone, at the ‘fault end’. On the basis of our analysis, we believe that the mainshock occurred at a depth range of 20–30 km at the base of the seismogenic zone, where 90% of aftershocks concentrated at this zone.

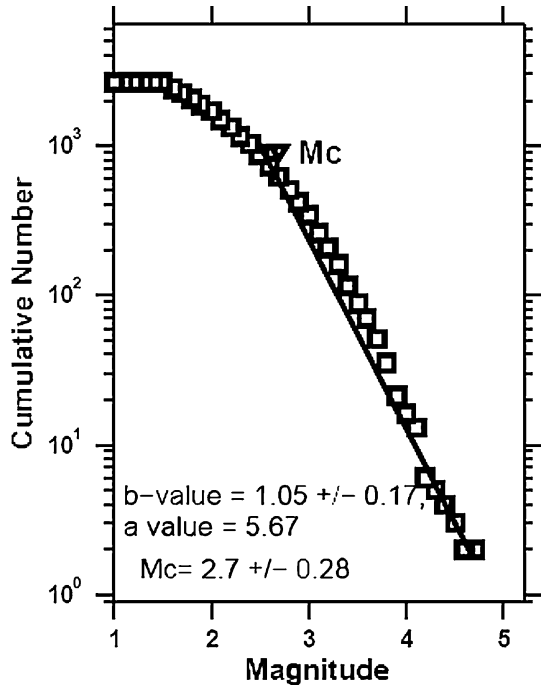
Further, the frequency–magnitude distribution of earthquake is well expressed by the Gutenberg–Richter relation (Gutenberg and Richter 1944),

$$\text{Log } (N) = a - bM \tag{1}$$

where ‘*N*’ is the number of events, ‘*M*’ is the magnitude, ‘*a*’ and ‘*b*’ are constants. From this relationship, it is found that the number of earthquakes declines logarithmically with the increase in the magnitude (Fig. 4). The extent of this decline is expressed by the ‘*b*-value’, which is normally close to 1. Studies of Mogi (1963) and Scholz (1968) reveal that the *b*-value depends on the percentage of existing stress within the rock sample of the final breaking stress. Also, it depends on the mechanical heterogeneity of the rock mass and increases with the increase in the heterogeneity. We have used improved catalog that contains accurate location information with error estimates in all three directions and local magnitude (*M_L*) estimates. For ‘*b*-value’ study, an *M* ≥ 2.7 catalog of Bhuj aftershocks is designed using combined hypocenter data from ISR and NGRI. Fitting above equation to the 3,850 aftershocks sequence of the 2001 Bhuj earthquake since August 2006 to October 2009 by using least square approach gives ‘*a*’ and ‘*b*’ as 5.67 and 1.015 ± 0.17, respectively. Studies of the tectonic earthquakes are characterized by the *b*-value from 0.5 to 1.5 and more frequently around 1.0 (Agrawal 1991; Mandal and Rastogi 2005), which is observed in the present study.

As mentioned previously, in order to use LET technique to assimilate 3-D velocity structures for different depth slices, we improved earlier earthquake epicenter and hypocenter location parameters determined by Hypo71 program (Lee and Lahr 1975), using the 1-D velocity model of Mandal (2007). The estimated 1-D velocity structure suggests an eight-layered crust beneath the region that is constrained by integrated geophysical results and controlled source seismic results (Kaila et al. 1990; Gupta et al. 2001). The integrated geophysical survey revealed a five-layered structure overlying the granitic basement (3–6 km), which consists of a high-velocity layer of Deccan basalts sandwiched between the Quaternary sediments and Jurassic sediments (Gupta et al. 2001). However, the results obtained from only single profile of controlled source seismic sounding close to the

Fig. 4 Plot showing *b*-value estimates from the events used in the study for the Kachchh region



aftershock zone suggest a Moho depth of 40–43 km and a variation from 37 to 45 km in most of the Kachchh region (Reddy et al. 2001). Further, the receiver transfer function analysis of teleseismic P-waves recorded at Bhuj station revealed a Moho thickness of 42 km and an upper mantle velocity of the order of 8.20 km/sec (Kumar et al. 2001). The same 1-D velocity model was used by Mandal (2007) for obtaining detailed 1-D travel time inversion for the 2001 Bhuj earthquake region.

4.1 Tomographic inversion

To analyze the arrival time data, we used the tomographic method of Zhao et al. (1992) to invert the arrival time data to determine the 3-D imaging of the velocity structure and Poissons's ratio. This method has been applied to many parts of the world in diverse tectonic environ. The inversion of arrival time data makes adjustment (perturbations) to a starting velocity model such that the difference between the predicted and the observed arrival times is minimized in the least square sense. The model space is divided into fine spaces by setting up a 3-D grid network, and the velocity perturbations are parameterized using values at grid nodes. Between grid nodes, the velocity perturbation at any point in the model is calculated by linearly interpolating the velocities at eight grid nodes surrounding that point. A continuous velocity perturbation field is then completely represented by the set of nodal values. The parameters to be determined are the velocity perturbation from the starting model at each grid node and four hypocenter parameters for each earthquake (latitude, longitude, depth, and origin time). Our velocity parameterization based on Zhao et al. (1992) approach is conspicuously different from the block parameterization as used in other 3-D local earthquake tomographic studies (Aki and Lee 1976; Aki et al. 1977). In the block approach, the earth is divided into many small blocks, each having uniform seismic

velocity values, which introduces artificial discontinuities at boundaries of different blocks. This issue of artifact has been addressed by Zhao et al. (1992) by adopting flexible grid parameterization during 3-D inversion of the travel time data set, in which they applied both Snell’s law and Pseudo-bending techniques to estimate perturbation in velocity values at points located at discontinuous and continuous layers, respectively. To calculate travel times and ray paths accurately and rapidly, we employed the 3-D ray tracing technique of Zhao et al. (1992), with station elevations taken into account. The nonlinear tomographic problem was solved by iteratively conducting linear inversions. At each iteration, perturbation to hypocenter parameters and velocities were determined simultaneously. Further details of the method were given by Zhao et al. (1992, 1994 and 2002).

A number of different grid spacing were tested. Though, from the resolution analyses for different grids, we found that a grid with a horizontal spacing of about 25 km and a vertical spacing of 5 km was adequate for the given distributions of seismic stations and earthquakes. We conducted rigorous tests for damping parameters (Fig. 5) for both P- and S-wave travel time inversions to obtain resolvable seismic structures, which are dictated by the number of hit counts at every grid. The damping parameter for the inversion was selected based on an empirical approach (Eberhart-Phillips 1986; Zhao et al. 1992). A number of inversions were carried out with different damping values for the selected 1-D velocity model to understand at what suitable damping the inversion can give the optimal residual reduction and the solution variance. The damping parameter was estimated by analyzing both data and solution variance with respect to the root mean square (RMS) travel time residuals (Fig. 5). We plot the trade of curves between the RMS and travel time residuals and the variance of the solution for both P- and S-wave velocities for different damping values. This shows under-damping below the damping value of 10 and

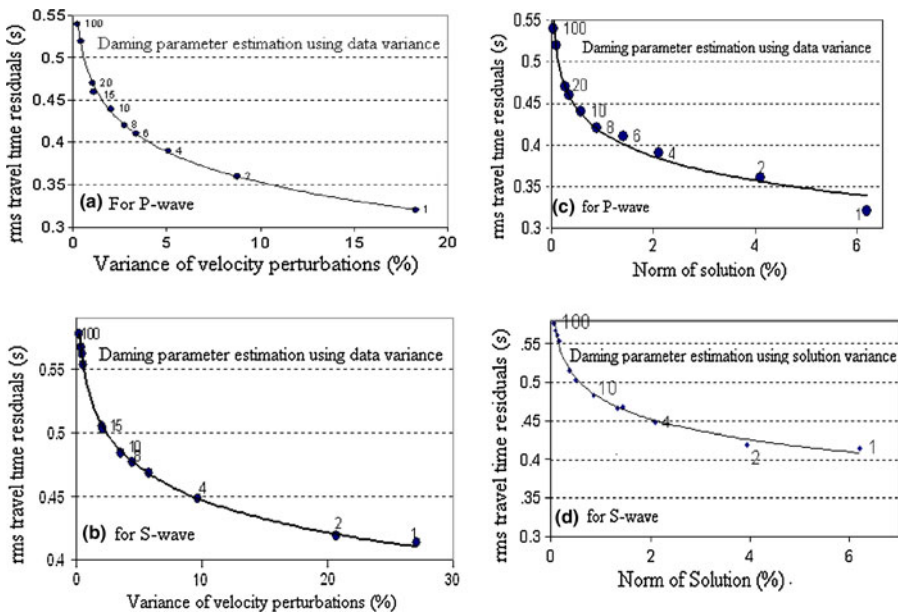


Fig. 5 Plots showing estimates of damping parameters for both P- and S-wave inversion using variance and norm of solution methods

over-damping above the value 10 (Fig. 5). On the basis of these analyses, we chose a damping of 10 for both P- and S-wave data inversion. This value gives convergent and consistent solution to our data set. We found that hit counts vary from 500 to 2000 at different depth layers around the 2001 Bhuj mainshock hypocenter (Fig. 6).

After obtaining the P- and S-wave velocity model as described earlier (Figs. 7, 8), the relation $(V_p/V_s)^2 = 2(1-\sigma)/(1-2\sigma)$ is used to determine the elastic parameter, Poisson's ratio (σ) (Utsu 1984), of structures at different layers as shown in Fig. 9. Their cross-sectional images are shown in Fig. 10. The Poisson's ratio (σ) is a key parameter in studying petrologic properties of crustal rocks and can provide tighter constraints on the crustal composition that cannot be well understood either by P- or S-wave velocity alone (Zhao et al. 2004). Its value in common rock types ranges from 0.20 to 0.25. Poisson's ratio has proved to be very effective for the clarification of the seismogenic behavior of the crust, especially the role of crustal fluids in the nucleation and growth of earthquake rupture (Zhao et al. 2002; Mishra and Zhao 2003).

Our assimilated 3-D seismic structures (V_p , V_s , and σ) as shown in Figs. (7, 8, 9, and 10) demonstrate that the region under investigation has strong crustal heterogeneities in both seismic velocity (V_p , V_s) and Poisson's ratio (σ).

4.2 Resolution tests

We conducted checkerboard resolution tests for both V_p and V_s seismic structures rigorously using checkerboard resolution test method of Zhao et al. (1992), originally derived from Humphreys and Clayton (1988) and Inoue et al. (1990) to examine the spatial resolution of the present data set. For this purpose, we have generated synthetic arrival time data from original (real) travel time data for both V_p and V_s structures. The synthetic arrival time data are generated by adding random Gaussian noise that varied from ± 0.1 to ± 0.2 , which were then inverted for the same model parameterization that was used for inverting the original data set. To make a checkerboard, the synthetic model is divided into alternating regions of positive and negative velocity anomalies of $\pm 3\%$ (Fig. 11) to be recovered in the solution models. Better recovery of alternate positive and negative anomalies after rigorous 3-D inversion of the synthetic data with original model parameterization indicates resolvable data set to infer how authentic simulated tomograms are for our interpretation in terms of geology and seismotectonics. Therefore, just seeing the image of the synthetic inversion of the checkerboard, one can soon understand where the resolution is good and where it is poor. The initial model used for the test is the same as that used for real inversion. Figures 12, 13 show the result of resolution test for both V_p and V_s wave velocities at 25-km grid spacing to assess the resolution of our data set. In this test, random error (0.1–0.15) having a normal distribution with a standard deviation of 0.15 was added to the synthetic data and same inversion algorithm as that for the real data was used. We found that the resolution is better near the surface and in the depth range of 20–25 km for 25-km horizontal and 5-km vertical resolutions; the test results show that the checkerboard pattern is well recovered alternatively for both V_p and V_s structures for all depth levels in and around the Bhuj mainshock hypocenter because of the concentration of a majority of aftershock events around the mainshock hypocenter that causes a high density of ray coverage at all depth as evident from hit count tests (Fig. 6). However, the velocity images (V_p , V_s) have also comparatively lesser resolution for velocity images assimilated for 15- and 30-km depth layers because of lesser number of events from these layers, reducing hit counts at these depths (Fig. 6).

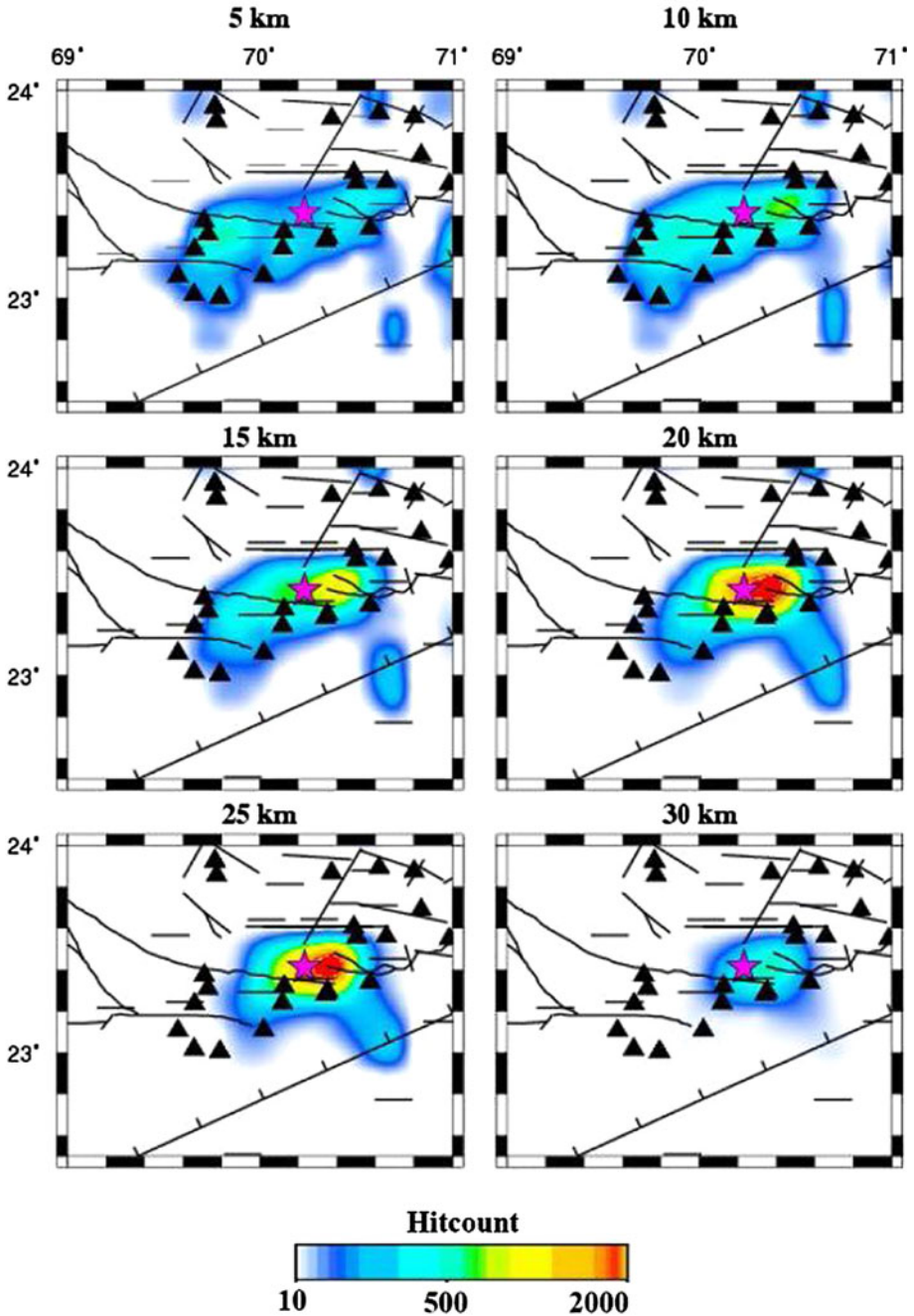


Fig. 6 Distribution of hit counts that represent number of rays passing through each grid node (hit count) for different depth layers, which is nearly same for both P- and S-wave data. The *star* shows 2001 Bhuj mainshock epicenter. Scale of hit count (blue: lesser hit counts; and red: higher hit counts) is shown below maps

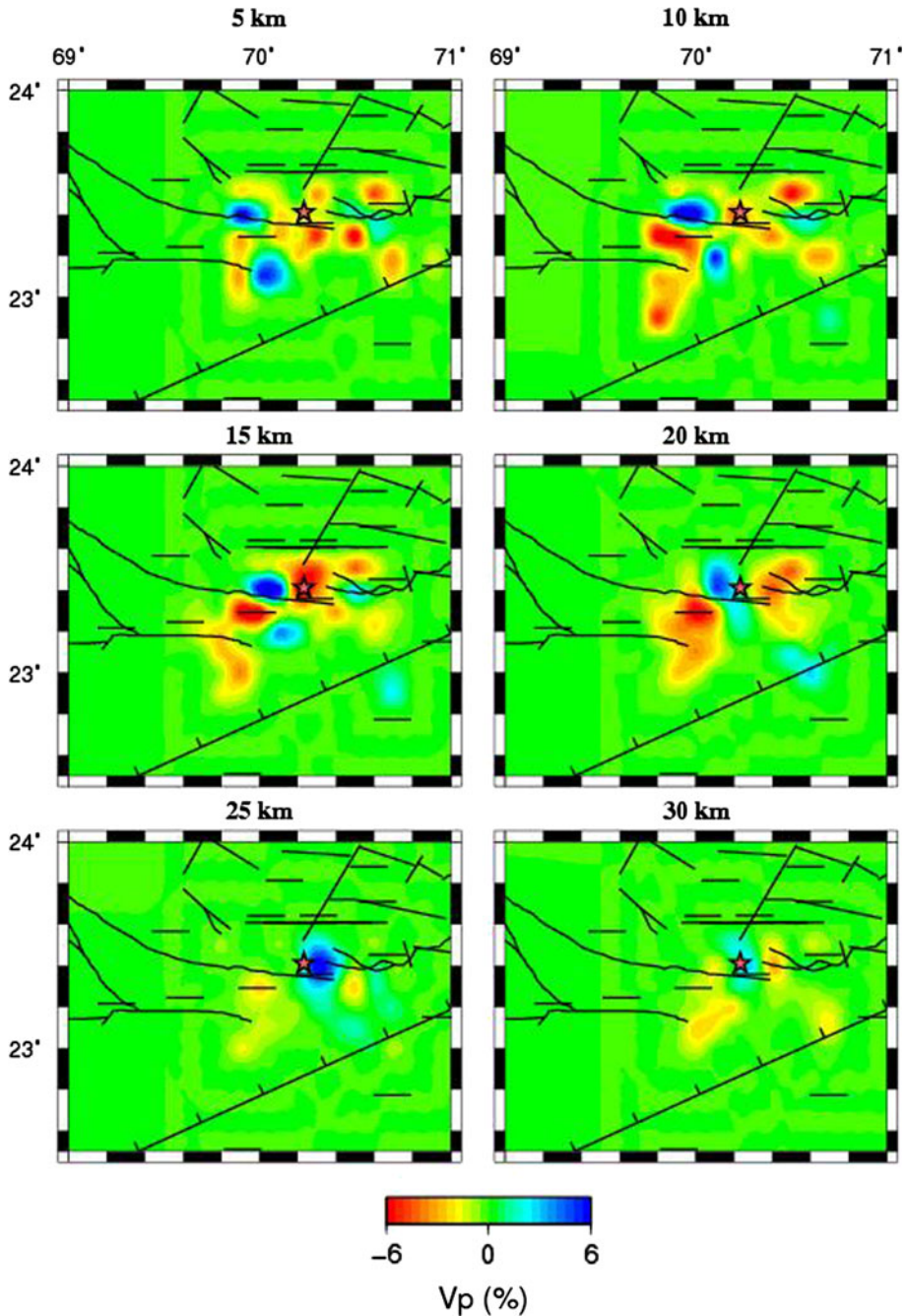


Fig. 7 P-wave velocity perturbation from the average velocity model in (%) at different depth layers beneath the 2001 Bhuj epicentral region. The scale of perturbation is shown at bottom. The red color denotes lowest perturbation, while blue color denotes highest perturbation from the average velocity model at specific depth layer. Colors indicate low and high velocities, respectively. The star indicates the mainshock of the Bhuj 2001. The figure also shows the identified faults of the regions. The perturbation scale is shown to the lower

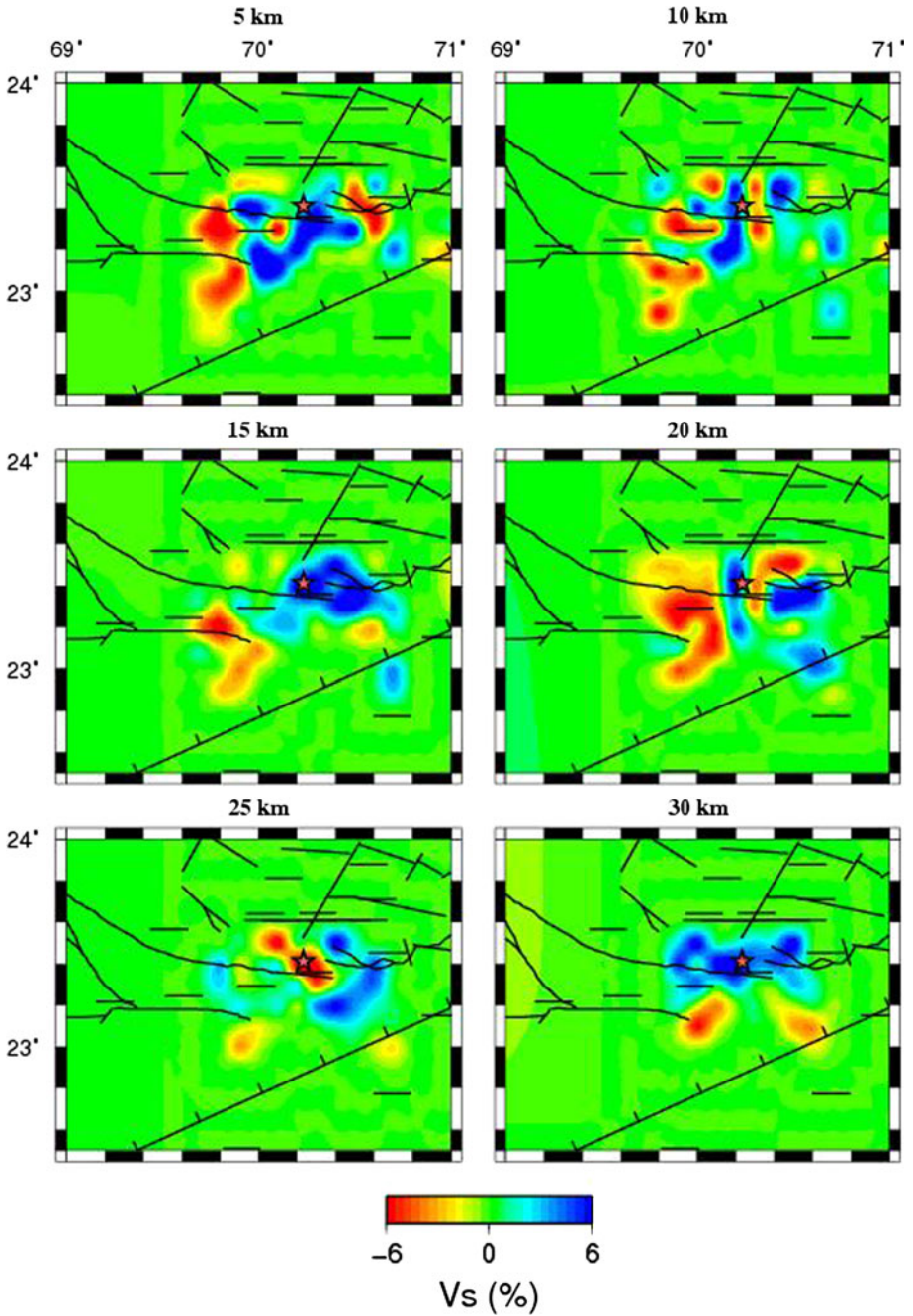


Fig. 8 S-wave velocity structures from the average velocity model (in %) at different depth layers beneath the Bhuj epicentral region. The *perturbation color scale* is same as shown in Fig. 7

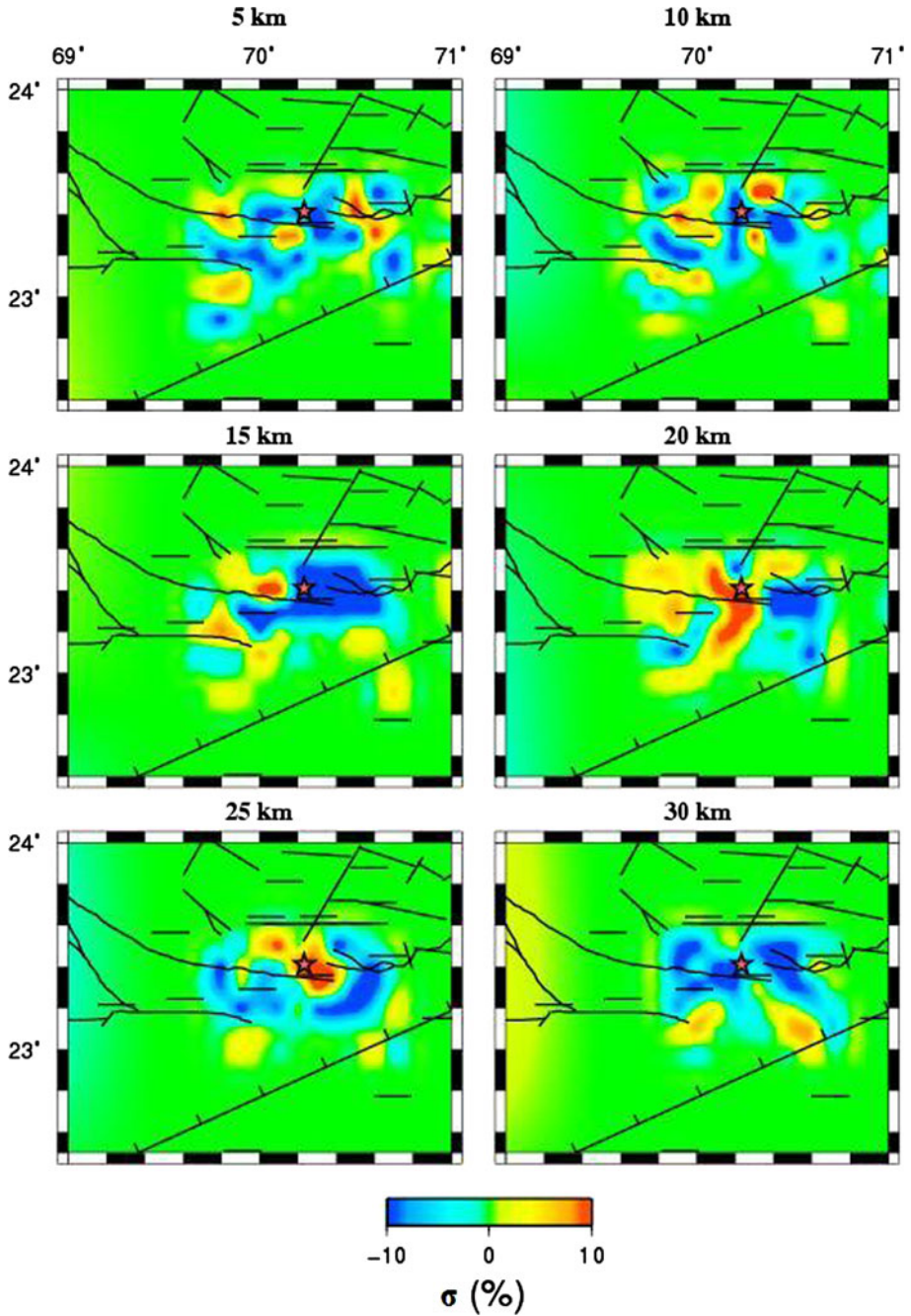


Fig. 9 Poisson's ratio (σ) structures estimated at different depth layers from 3-D perturbed values of P- and S-wave velocity at corresponding depth layers (in %) beneath the Bhuj epicentral region. The scale of σ -perturbation is shown in color at the bottom. The red color denotes higher perturbation in σ , while blue color denotes its low perturbation

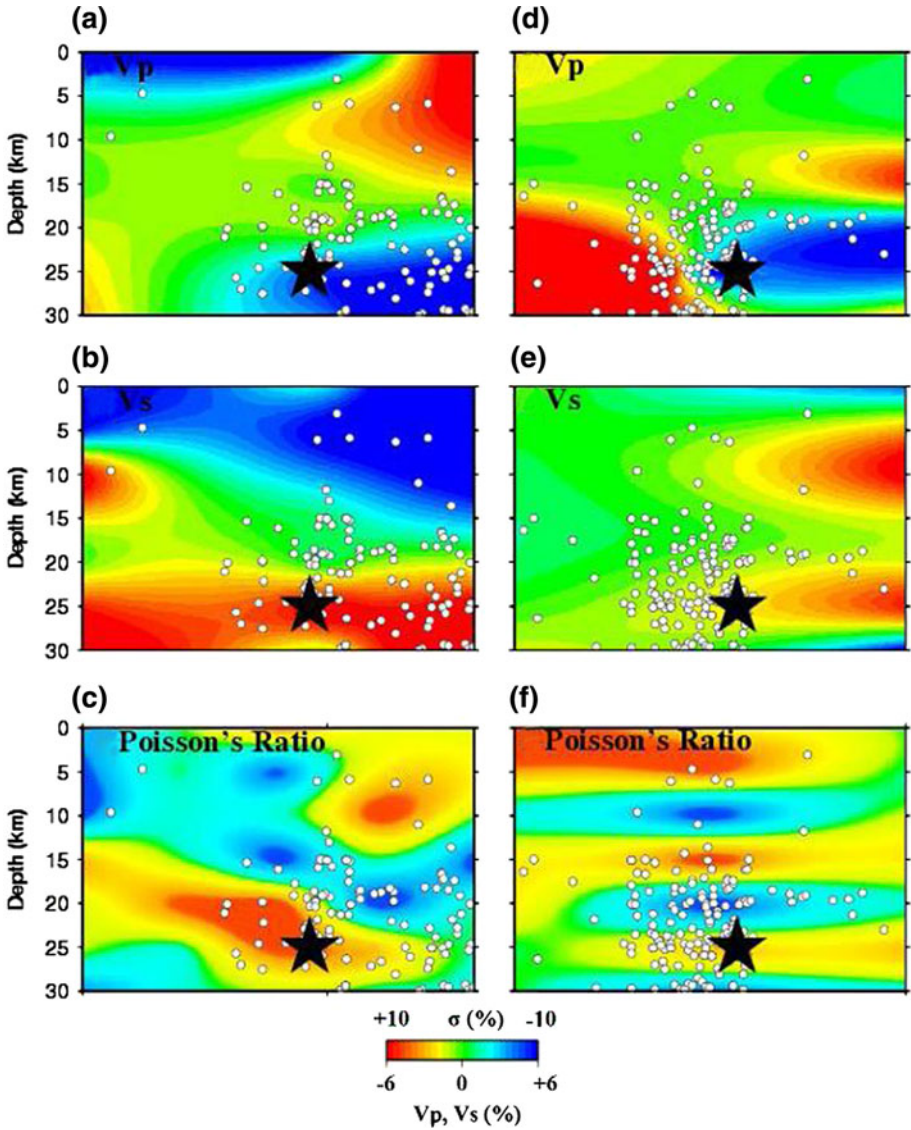


Fig. 10 Maps showing cross-sectional views of distribution of V_p , V_s , and σ with depths along *two lines*: AB and CD as sketched in Fig. 1a. The *upper two* indicate V_p , middle V_s and last two σ . The perturbation (in %) scale in color is shown at the *bottom*

5 Interpretations and discussion

Applying the tomographic method to our relocated data sets and adopting the initial velocity model as described earlier, we obtained a convergent and consistent solution after three iterations. The RMS travel time residual was deduced from 0.50227 to 0.32674 s for P-wave and from 0.58220 to 0.37301 s for S-wave inversions. The results of the 3-D V_p , V_s and σ distributions at 5-km depth intervals (5–30 km) are shown in Figs 7, 8, 9, and 10.

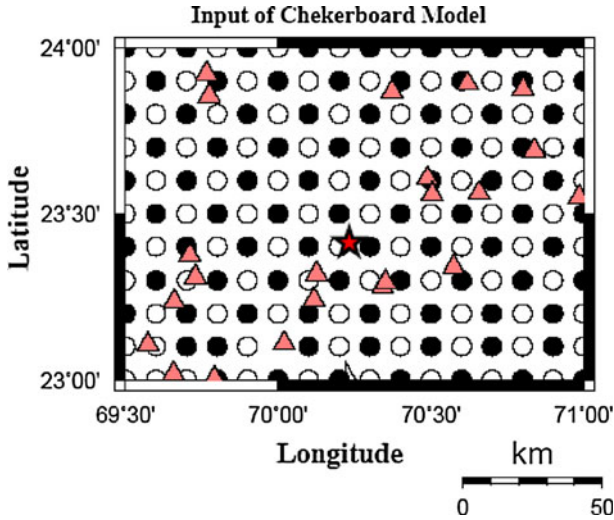


Fig. 11 The map shows input synthetic model for conducting checkerboard resolution tests for both P- and S-wave by introducing perturbation at every grid in the modeling space of $\pm 3\%$. The dark and open white circles at every grid node denote negative and positive perturbation of 3%, respectively

Significant variations in the velocity up to 6% and Poisson's ratio up to 10% are revealed in the surrounding area. The tomographic images for V_p , V_s and σ show a consistent result at depths of 5–15 km (Figs. 7, 8, 9, and 10). The V_p and V_s images (Figs. 7, 8) show an alternate low- and high-velocity zones while the σ imaging (Fig. 9) depicts a low Poisson's ratio structure at the above-mentioned depths. At shallower depth (0–5 km), the low V_p and low V_s may indicate the presence of soft and thick alluvial sediments with higher water content around the North Wagad Fault (NWF) probably on its hanging wall. Generally, the V_p - and V_s -imaged region corresponds to the high seismicity region, close to the fault plane, for the western part of the aftershock area. On the other hand, where aftershocks are concentrated in the eastern region, there are relatively high σ values. The images of V_p , V_s and σ at depths of 20 and 25 km reveal very interesting structures (Figs. 7, 8, 9) because of sensitivity of imaged crustal heterogeneities with depths. It is also interesting to note that above the 2001 Bhuj mainshock hypocenter at 20-km depth showed high V_p , high σ , and these high anomalous bodies at 20-km depth is flanked by two prominent low V_p and low σ on either side of it below 20-km depth of the 2001 Bhuj mainshock hypocenter (Figs. 7, 9). V_s images (Fig. 8) also show similar patterns at the depths. It means the fault zone of the mainshock hypocenter is flanked with a considerable amount of structural heterogeneity. So, the degree of cohesive forces at 20-km depth on either side of the mainshock is different due to different seismic strength of the fault segments (Mishra and Zhao 2003). Very close to the mainshock hypocenter, the zone at 25-km depth is associated with high V_p , low V_s and high σ values (Figs. 7, 8, and 9), where most of the aftershocks are also located. Such an anomaly can be noted for the existence of a fluid-filled, fractured rock matrix (Mishra and Zhao 2003; Mandal et al. 2004a; Mandal and Pujol 2006; Mandal and Chadha 2008).

Zhao and Negishi (1998) inferred fluid-filled fractured rock matrix contribution for initiation of the large earthquakes. It is reasonable to consider fluid inclusion and degree of saturation of the causative source zone may be the plausible cause of influencing the

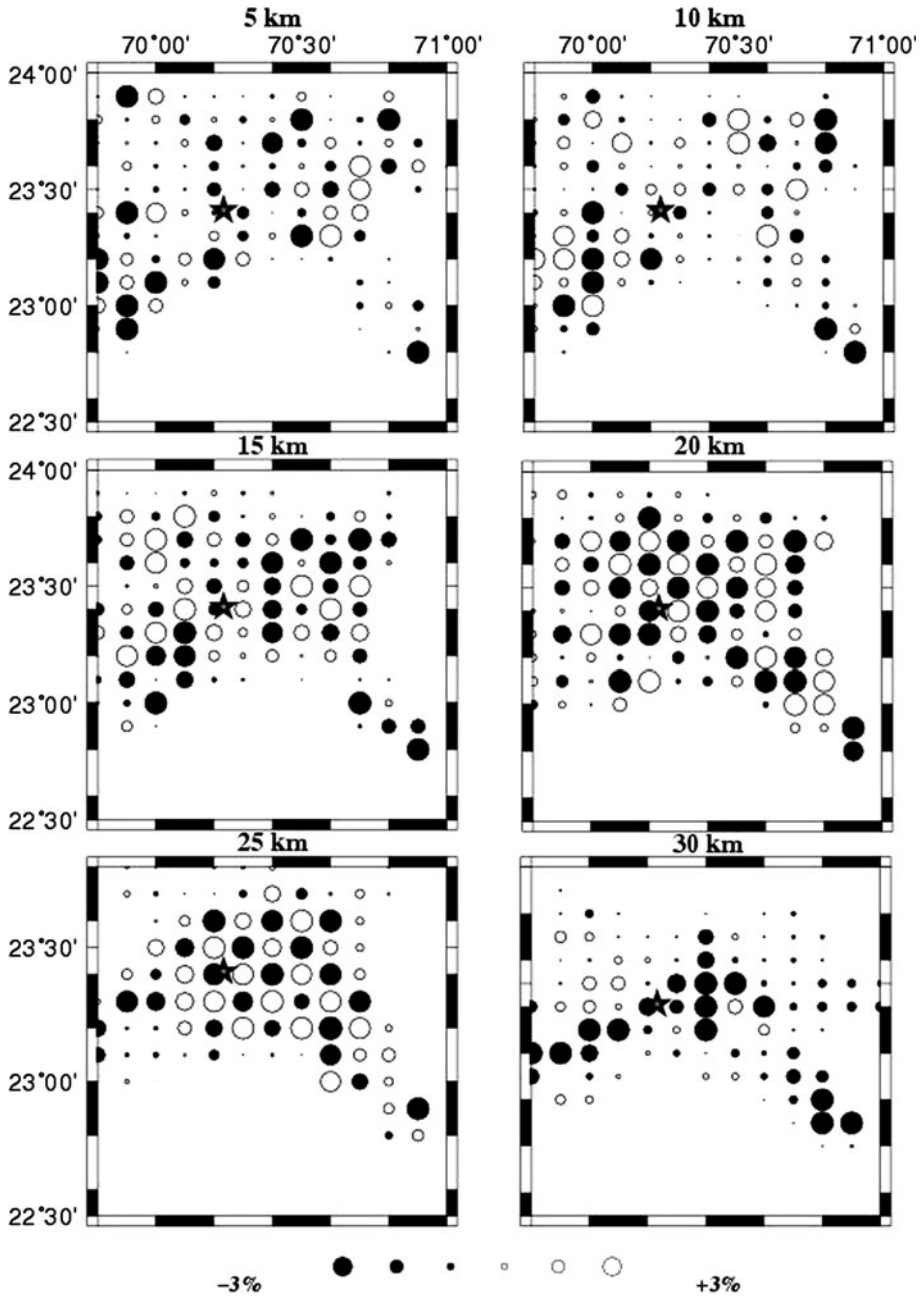


Fig. 12 The results of the checkerboard resolution test for P-wave velocity at six crustal depths. *Black and white circles* denote low and high velocities, respectively. The *perturbation scale* is shown at the bottom. The depth of each layer is shown at the upper middle of each map

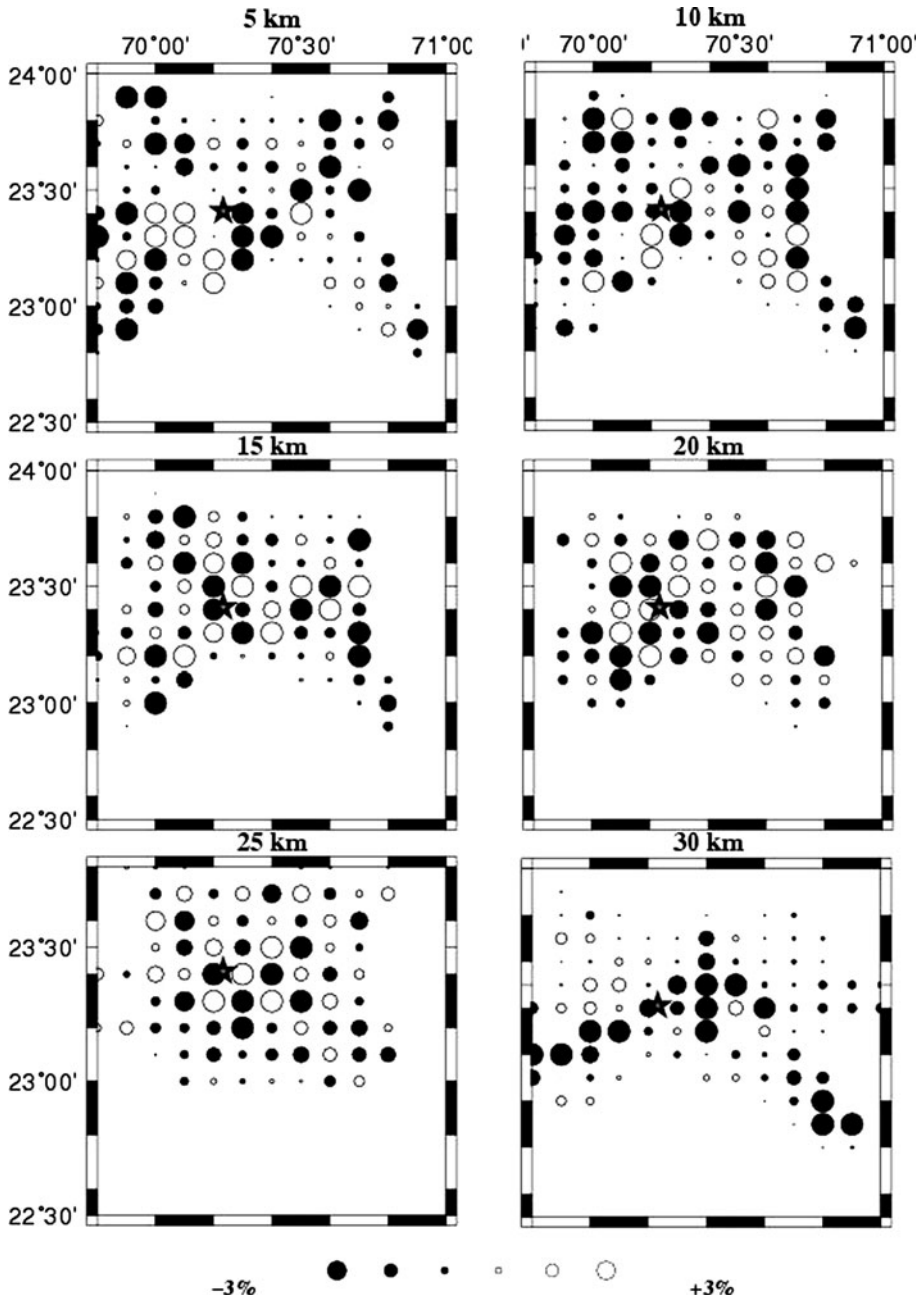


Fig. 13 The results of the checkerboard resolution test for S-wave velocity at six crustal depths. *Black and white circles* denote low and high velocities, respectively. The *perturbation scale* is shown in lower. The depth of each layer is shown at the upper middle of each map

seismogenic strengths on either side of the 2001 Bhuj mainshock (20 km) overlying the mainshock hypocenter (25 km).

Earlier studies (Kayal et al. 2002; Mishra and Zhao 2003; Mishra et al. 2008) of limited aftershock data recorded during January 29, 2001,–April 30, 2001, have noted 1) the 2001 Bhuj source zone at 20-km depth was associated with high V_p , high σ to the west and low V_p and low σ to its east. While higher V_s value was imaged to the east of the mainshock at this depth and 2) the source zone at 25-km depth was associated with high V_p , low V_s and high σ values where most of the aftershocks were located. However, tomographic studies for the same region by Mandal and Pujol (2006) and Mandal and Chadha (2008) investigated few patches of low V_p and V_s and high σ between 10 to 30 km on the 45° south dipping north Wagad fault, which was the causative fault for the 2001 Bhuj mainshock. Based on the considerable amount of structural heterogeneities as reflected in velocity and Poisson's ratio imaging results, they suspected seismic strength variation on either side of the mainshock at 20-km depth. An examination of the results of the previous limited data set and the present detailed study based on detailed autopsy of the 2001 source zone with comparatively large number of high-quality aftershock data recorded by more seismograph stations for longer duration (November 2006–April 2009) provides potential information of the sub-surface crustal physio-chemical properties of the source zone. Since 3-D seismic imaging represents dynamic snapshots of the sub-surface layers, reflecting the cumulative past geological changes within the host rocks till the data recorded in seismic imaging (Zhao et al. 2002). We infer that the 2001 Bhuj source zone may have undergone high degree of fluid saturation with lapse of about 8 years of the time from the occurrence of the January 26, 2001, Bhuj earthquake (Mw 7.6). Consequently, the several seismogenic faults and sub-surface cracks in the geologically older KRB is likely to get reinforced due to continuous occurrences of micro- to moderate earthquakes in the source region since the 2001 Bhuj. This in turn may have provided suitable environs for fluid dynamics in the cracked volume of the sub-surface rock matrix beneath the 2001 Bhuj mainshock. These observations suggest that changes in seismic strength beneath the source zone by inclusion of fluids and saturation of host rock matrix are likely to dictate and hence influence genesis of micro- to macro-earthquakes in the region for years and creating panic among the local people. Presence of fluids beneath the 2001 Bhuj and the 1993 Latur-Killari mainshock hypocenters has also been deciphered by observing high conductivity from magnetotelluric investigations (Arora et al. 2002; Gupta et al. 1996) and low Bouguer anomaly from gravity investigation in the Bhuj area due to mass deficiency caused by fluid-filled fractured/cracked rock matrix at the mainshock hypocenter depth (Chandrashekhar and Mishra 2002). The high b -value (>1.0) estimate (Fig. 4) from the present data set suggests existence of strong 2-D heterogeneity present in the source area.

Based on above results, it is reasonable to consider fluid inclusion at 20–25-km depth, which might have triggered the 2001 Bhuj earthquake and facilitated the nucleation of the present-day micro-tremors in the region. Paleo-seismicity studies of the region indicated that earthquakes in KRB had contributed to relaxation of high ambient stresses that got locally concentrated within the rheological heterogeneities. The rheological heterogeneities may be due to intruded igneous complexes of the Deccan volcanic plugs, crustal thinning and thickening processes, fractured fluid-filled rock matrix, and mafic intrusive with structural uplifts related to the convergence of the Kachchh rift basin. The mafic intrusive may be related to the Deccan trap activity or to some older activity related to the convergence of the Kachchh rift basin (Mishra et al. 2008). The area of low V_s and high σ values can be seen in the depth range of 30 km beneath the mainshock hypocenter. The V_s image is different from V_p image (Figs. 7, 8, and 10) and S-waves are much sensitive to

the fluid content in the material than P-waves (Zhao and Negishi 1998). These features are similar to the velocity anomalies in the hypocenter region of the 1995 Kobe earthquake region (Zhao et al. 1996), the 2000 Tottori earthquake (Zhao et al. 2004) and the 1993 Latur-Killari earthquake (Mukhopadhyay et al. 2006).

The source of fluids at the 2001 mainshock hypocenter may be due to many reasons, such as dehydration of hydroxyl-bearing rocks of the crustal and sub-crustal layers; permeation of meteoric or sea water through active faults or fractures connected to the mainshock source zone; or existence of Paleo-fluids in the Paleo-rift zones having intersecting fault geometries. It is intriguing to note that the 2001 Bhuj mainshock was located near a triple junction that is formed between intersections of three important tectonic plates, such as Indian, Arabian and Iranian plate (Fig. 1b) that may have reinforced the degree of fracture or enhancement of cracks beneath the sub-surface just as that of Mendicino-triple junction located very near to San-Andreas fault where the great 1906 San-Francisco earthquake occurred. The source zone is also connected to the geologically older Owen Fracture zone of about 65 Ma from the Arabian Sea that may have great influence on structural heterogeneities of the 2001 Bhuj earthquake source zone, contributing to the development of differential strain at the mainshock hypocenter.

Detailed information on sub-surface causative seismogenic faults is essentially required as inputs for evolving a comprehensive model for earthquake risk mitigation for a region. The generation of a shallow crustal earthquake could be controlled by a deep process in the lower crust and upper mantle. From this point of view, it is vital to investigate the detailed structure and processes of the lower crust and upper mantle for clarifying the seismogenesis and reducing earthquake risk. It is insufficient to refer only to the surface description of active faults to predict seismic potential of a region. Note that field survey did not find any fault traces on the surface in the focal areas of the 2001 Bhuj earthquake and the 2000 Tottori earthquake, Japan (Shibutani et al. 2002). The 1993 Latur-Killari earthquake had also not resulted in any of the surface faults trace on the surface (Mukhopadhyay et al. 2006). It is also found that there are no mapped faults or obvious topographic features in the 2001 Bhuj focal area (Negishi et al. 2002; Kayal et al. 2002; Mishra and Zhao 2003; Mandal et al. 2004a; Mandal and Pujol 2006; Mandal and Chadha 2008), which occurred on buried fault extending from 8-km to 35-km depth. Occurrence of Bhuj, Latur-Killari, and Tottori earthquakes are almost hidden faults is very important aspect for evaluation of seismic or earthquake hazards. Large damaging earthquakes can occur on buried faults that leave very little surface evidence of faulting that can be used to identify past earthquakes. We infer that the use of detailed 3-D seismic tomography may offer potential information on hidden and unmapped faults beneath the plate interior to unravel what and how the genesis of such big damaging earthquakes caused. This study may help in evolving a comprehensive earthquake hazard mitigation model for a region. Inferences of the present study may be used for regions of analogous geotectonic settings for evaluating earthquake hazards and evolving its earthquake hazard mitigation model.

6 Conclusions

In this study, a detailed autopsy of the 2001 Bhuj earthquake source zone has been carried out by conducting 3-D seismic velocity and Poisson's ratio imaging method of Zhao et al. (1992) by inverting a large quantity of high-quality arrival time data of P- and S-wave generated from a total of 576 local earthquakes recorded between November 2006 and April 2009 by a seismic network consisting of 22 three-component broadband digital

seismograph stations ascribing to the Institute of Seismological Research (ISR), Gandhinagar, Gujarat, and NGRI, Hyderabad, India. Our tomographic results are generally consistent with previous geophysical observations ascribing to the characteristics of seismotectonically active regions. It was surprising that the large damaging earthquake located in the deeper crust did not have surface faulting. The fault plane is small and steep. Our results provide information for imaging the source area and understanding the reholological causes of this earthquake. It is also interesting to note that the mainshock hypocenter is associated with high V_p , low V_s high σ at 25-km depth where most of the aftershocks are also located. Results of the synthetic and checkerboard anomalies indicate that the reliable features are down to a depth of 25 km. Such an anomaly possibly indicates the existence of a fluid-filled, fractured rock matrix, which may have contributed to the initiation of the large earthquakes. We infer that the use of the detailed 3-D seismic tomography may offer potential information on hidden and unmapped faults beneath the plate interior to unravel the genesis of such big damaging earthquakes. This study may help in evolving a comprehensive earthquake risk mitigation model for a region. Inferences of the present study may be used for regions of analogous geotectonic settings for evaluating earthquake hazards and evolving its earthquake risk mitigation model.

Acknowledgments The authors are grateful to the NGRI for providing aftershock data for the study. OPM is thankful to Director General, Geological Survey of India, for permission and encouragement to conduct such studies for the benefit of science and society. This work is partially supported by Gujarat State Disaster Management Authority (GSDMA) and Ministry of Earth Science, New Delhi .

References

- Agrawal PN (1991) Engineering seismology. Oxford and IBH Publishing Co Pvt Ltd, New Delhi
- Aki K, Lee WHK (1976) Determination of the three dimensional velocity anomalies under a seismic array using first P arrival times from local earthquakes I A homogeneous initial model. *J Geophys Res* 81:4381–4399
- Aki K, Christofferson A, Husebye E (1977) Determination of the three-dimensional seismic structure of the lithosphere. *J Geophys Res* 82:277–296
- Arora BR, Rawat G, Singh AK (2002) Mid-crustal conductor below the Kutch Rift and its seismogenic relevance to the 2001 Bhuj earthquake. *DCS—DST News Govt. of India New Delhi, India* 22–24
- Biswas SK (1987) Regional framework, structure and evaluation of the western marginal basins of India. *Tectonophysics* 135:302–327
- Bureau of Indian Standards (2002) Criteria for earthquake resistant design of structures (fifth revision), pp 39
- Chandrasekhar DV, Mishra DC (2002) Some geodynamic aspects of Kutch basin and seismicity: an insight from gravity studies. *Curr Sci* 83:492–498
- Chung WY, Gao H (1995) Source parameters of the Anjar earthquake of July 21, 1956, India, and its seismotectonic implications for the Kachchh rift basin. *Tectonophysics* 242:281–292
- Eberhart-Phillips D (1986) Three dimensional velocity structure in northern California coast ranges from inversion of local earthquake arrival times. *Bull Seism Soc Am* 76:1025–1052
- Gaur VK (2001) The Ran of Kachchh earthquake, 26 January 2001. *Curr Sci* 80(3):336–340
- Gorbatov A, Kennett BLN (2003) Joint bulk-sound and shear tomography for western Pacific subduction zones. *Earth Planet Sci Lett* 210:527–543
- Gupta HK, Sarma SV, Harinarayana T, Virupakshi G (1996) Fluids below the hypocentral region of Latur earthquake, India: geophysical indicators. *Geophys Res Lett* 23:1569–1572
- Gupta HK, Harinarayana T, Kousalya M, Mishra DC, Mohan I, Rao NP, Raju PS, Rastogi BK, Reddy PR, Sarkar D (2001) Bhuj earthquake of 26 January 2001. *J Geol Soc India* 57:275–278
- Gutenberg B, Richter CF (1944) Frequency of earthquakes in California. *Bull Seism Soc Am* 34:185–188
- Humphreys E, Clayton R (1988) Adaptation of back projection tomography to seismic travel time problems. *J Geophys Res* 93:1073–1085

- Inoue H, Fukao Y, Tanabe K, Ogata Y (1990) Whole mantle P wave travel tomography. *Phys Earth Planet Inter* 59:294–328
- Johnston AC (1994) Seismotectonic interpretations and conclusions from the stable continental regions. In: the earthquake of stable continental regions: Assessment of large earthquake potential. Electric Power and Research Institute, Palo Alto, Report TR 10261
- Kaila KL, Tewari HC, Krishna VG, Dixit MM, Sanker D, Reddy MS (1990) Deep Seismic sounding studies in the north Cambay and Sanchar basin, India. *Geophys J Int* 103:621–637
- Kayal JR, Zhao D, Mishra OP, De R, Singh OP (2002) The 2001 Bhuj earthquake: tomographic evidence for fluids at the hypocenter and its implications for rupture nucleation. *Geophys Res Lett* 29(24):2152
- Kumar MR, Saul J, Sarkar D, Kind R, Shukla AK (2001) Coastal structure of Indian shield: new constraints from teleseismic receiver function. *Geophys Res Lett* 28:1339–1342
- Lay T, Wallace TC (1995) *Modern global seismology*. Academic Press, San Diego, California, pp 521
- Lee W, Lahr J (1975) HYPO71 (revised): a computer program for determining hypocenter, magnitude, and first motion pattern of local earthquakes. US: Geol Surv: Open-File-Report 75–311, pp 114
- Mandal P (2007) Sediment thicknesses and Qs vs. Qp relations in the Kachchh rift basin, Gujarat, India using Sp converted phases. *Pure Appl Geophys* 164:135–160
- Mandal P, Chadha RK (2008) Three-dimensional velocity imaging of the Kachchh seismic zone, Gujarat, India. *Tectonophysics* 452:1–16
- Mandal P, Pujol J (2006) Seismic imaging of the aftershock zone of the 2001 Mw 7.7 Bhuj earthquake, India. *Geophys Res Lett* 33:L05309. doi:10.1029/2005GL025275
- Mandal P, Rastogi BK (2005) Self-organized fractal seismicity and b value of aftershocks of the 2001 Bhuj earthquake in Kutch (India). *Pure Appl Geophys* 162:53–72
- Mandal P, Rastogi BK, Satyanarayana HVS, Kousalya M (2004a) Results from local earthquake velocity tomography: implications toward the source process involved in generating the 2001 Bhuj earthquake in the lower crust beneath Kachchh (India). *Bull Seism Soc Am* 94(2):633–649
- Mandal P, Rastogi BK, Satyanarayana HVS, Kousalya M, Raghavan R, Satyamurthy C, Raju IP, Sarma ANS, Kumar N (2004b) Characterization of causative fault system for 2001 Bhuj earthquake of Mw 7.7. *Tectonophysics* 378:105–121
- Mishra OP, Zhao D (2003) Crack density, saturation rate and porosity at the 2001 Bhuj, India, earthquake hypocenter: a fluid-driven earthquake? *Earth Planet Sci Lett* 21:393–405
- Mishra OP, Zhao D, Wang Z (2008) The genesis of the 2001 Bhuj, India earthquake (Mw 7.6): a puzzle for Peninsular India? *Spel Issue Indian Minerals* 61(3 & 4):149–170
- Mogi K (1963) Some discussion on aftershocks and earthquake swarms—the fracture of a semi infinite body caused by an inner stress origin and its relation to the earthquake phenomena. *Bull Earthq Res Inst* 41:615–658
- Mukhopadhyay S, Mishra OP, Zhao D, Kayal JR (2006) 3-D Seismic structure of the source area of the 1993 Latur, India earthquake and its implications for rupture nucleations. *Tectonophysics* 415:1–16
- Negishi H, Mori J, Sato T, Singh R, Kumar S, Hirata N (2002) Size and orientation of the fault plane for the 2001 Gujarat, India earthquake (Mw 7.6) from aftershocks observations: a high stress drop event. *Geophys Res Lett* 29:1949. doi:10.1029/2002GL015280
- Rajendran CP, Rajendran K (2001) Character of deformation and past seismicity associated with the 1819 Kachchh earthquake, northwestern India. *Bull Seismol Soc Am* 91(3):407–426
- Rajendran K, Rajendran CP, Thakkar MG, Tuttle MP (2001) The 2001 Kutch (Bhuj) earthquake: coseismic surface features and their significance. *Curr Sci* 80:1397–1405
- Rastogi BK, Gupta HK, Mandal P, Satyanarayana HVS, Kousalya M, Raghavan RV, Jain R, Sarma ANS, Kumar N, Satyamurthy C (2001) The deadliest stable continental region earthquake that occurred near Bhuj on 26 January 2001. *J Seism* 5:600–615
- Reddy PR, Sarkar D, Sain K, Mooney WD (2001) Report on collaborative scientific study at USGS, Melno park, USA (30 October–31 December 2001), p 19
- Salah MK, Zhao D (2003) 3-D seismic structure of Kii Peninsula in southwest Japan: evidence for slab dehydration in the forearc. *Tectonophysics* 364:191–213
- Salah MK, Sahin S, Destici C (2007) Seismic velocity and Poisson's ratio tomography of the crust beneath southwest Anatolia: an insight into the occurrence of large earthquakes. *J Seism* 11:415–432
- Scholz CH (1968) The frequency–magnitude relation of microfracturing in rock and its relation to earthquakes. *Bull Seismol Soc Am* 58:399–415
- Serrano I, Morales J, Zhao D, Torcal F, Vidal F (1998) P-wave tomographic images in the central Betics-Alboran sea (South Spain) using local earthquakes: contribution for a continental collision. *Geophys Res Lett* 25(21):4031–4034
- Sibson RH (1989) Earthquake faulting as a structural process. *J Struct Geol* 11:1–14

- Talwani P, Gangopadhyay A (2001) Tectonic framework of the Kachchh earthquake of January 26, 2001. *Seismol Res Lett* 72:336–345
- Thurber CH (1983) Earthquake locations and three dimensional crustal structure in the Coyote Lake area, central California. *J Geophys Res* 88:8226–8236
- Utsu T (1984) Estimation of parameters for recurrence models of earthquakes. *Bull Res Inst Univ Tokyo* 59:53–66
- Widiyantoro S, Kennett BLN, Van der Hilst RD (1999) Seismic tomography with P and S-data reveals lateral variations in the rigidity of deep slabs. *Earth Planet Sci Lett* 173:91–100
- Zhao D, Kanamori H (1992) P-wave image of the crust and uppermost mantle in southern California. *Geophys Res Lett* 19:2329–2332
- Zhao D, Negishi H (1998) The Kobe earthquake: seismic image of the source zone and its implications for the rupture nucleation. *J Geophys Res* 103:9967–9986
- Zhao D, Hasegawa A, Horiuchi S (1992) Tomographic imaging of P and S wave velocity structure beneath northeastern Japan. *J Geophys Res* 97:19909–19928
- Zhao D, Hasegawa A, Kanamori H (1994) Deep structure of Japan subduction zone as derived from local, regional and teleseismic events. *J Geophys Res* 99:22313–22329
- Zhao D, Kanamori H, Negishi H, Wiens D (1996) Tomography of the source area of the 1995 Kobe earthquake: evidence for fluids at the hypocenter? *Science* 274:1891–1894
- Zhao D, Wang K, Rogers G, Peacock S (2001) Tomographic image of low P velocity anomalies above slab in northern Cascadia subduction zone. *Earth Planets Space* 53:285–293
- Zhao D, Mishra OP, Sanda R (2002) Influence of fluids and magma on earthquakes: seismological evidence. *Phys Earth Planet Inter* 132:249–267
- Zhao D, Tani H, Mishra OP (2004) Crustal heterogeneity in the 2000 western Tottori earthquake region: effects of fluids from slab dehydration. *Phys Earth Planet Inter* 145:161–177